
Mathematical Statistics
Stockholm University

# A Bayesian Simulation Study Using MCMC to Find Possible Ice Shelves Characteristics in the Arctic Ocean about 140 000 Years Ago

Carina Sundström

**Examensarbete 2012:5**

## Postal address:
Mathematical Statistics
Dept. of Mathematics
Stockholm University
SE-106 91 Stockholm
Sweden

## Internet:
http://www.math.su.se/matstat

Mathematical Statistics
Stockholm University
Examensarbete **2012:5**,
http://www.math.su.se/matstat

# A Bayesian Simulation Study Using MCMC to Find Possible Ice Shelves Characteristics in the Arctic Ocean about 140 000 Years Ago

Carina Sundström*

October 2012

**Abstract**

The aim of this thesis is to investigate possible features of ice shelves in the Arctic about 140000 years ago. The ice shelves have a critical role in the global climate system and since the human carbon emissions will increase the temperature in the future it is important to understand more about how the ice sheet interacts with the global climate. Today most ice shelves are found in the Antarctic. The Antarctic data are being used as plausible relations between several parameters under the presumption that the ice shelves in the Antarctic today have similar features as ice shelves in the Arctic 140000 years ago. Seafloor findings suggest that the Arctic has been covered with huge ice shelf complexes. Markov Chain Monte Carlo, MCMC, is a general simulation method that draws values from approximate distributions. The Markov chain used here is the Gibbs sampler and the software OpenBUGS has been performing the simulations. The results suggest that huge ice shelf complexes were extreme events but support the idea of ice shelves in the Arctic in the past.

*Postal address: Mathematical Statistics, Stockholm University, SE-106 91, Sweden. E-mail: carina_sundstrom@hotmail.com. Supervisor: Gudrun Brattström.

# 1 Table of Contents

# 2 Introduction

### 2.1.1 Ice Shelves

Ice shelves develop when grounded inland ice masses reach the coast and become afloat on the ocean. Today most ice shelves are found along the Antarctic coast line. Research suggests that there have been huge ice shelf complexes covering large parts of the Arctic Ocean, fed by large ice masses on the surrounding continental land masses and high Arctic Archipelago. Ice shelves are dynamic and undergo extremely slow creeping motions due to the action of gravity and in response to climate. The ice shelves have a critical role in the global climate system; if their feeding inland ice masses melt, sea level will rise. Therefore more ice shelf research have been performed since the mid 1970'ies (Kirchner et al. [2011]).

A very important part of the climate system is the ice sheets. Still they are among the least understood. In the past there have been dramatic changes to the global climate which was affected by the evolution of large ice sheets. The human carbon emissions will increase the temperature on earth in the future and it is important to understand how the ice sheet interacts with the climate. Increases in atmospheric or ocean temperatures might lead to thresholds on ice sheet stability being surpassed and the earth could become irreversibly committed to near-permanent ice sheet decay or sea level rise. What this would mean to humanity is not fully understood (Fyke et al. [2011]).

### 2.1.2 Seafloor Erosion From Ice Shelves

Large parts of polar continental margins and some submarine ridges in the central Arctic Ocean have been impacted by ice sheets and, occasionally by grounding ice sheets. Images of those impacted seafloors are important to our understanding of the history of these ice sheets. In the last years there have been new advances in geophysical mapping technologies which provide even clearer views of the seafloor. The reconstruction of the history and dynamics of ice masses in the Arctic Ocean are so far poorly understood. There is a hypothesis of a thick floating ice shelf over the entire Arctic Ocean in the Pleistocene. More analysis is needed to test this and other hypotheses.

In the Arctic Ocean there are dramatic changes between glacial and interglacial periods. The ice and melt-water discharge from the ice sheets had a high impact on the Arctic Ocean circulation and sedimentation regimes. Seafloor mapping data indicate glacial erosion at depths reaching 1000 meters below the sea level. There is convincing evidence that eroded areas of Lomonosov Ridge and Chukchi Borderland depicts a dramatic impact of large ice masses that once invaded the central Arctic Ocean from both the Laurentide (over present

areas of Canada) and Eurasian ice sheets. Seafloor features in the polar areas are ice keel scours, also called plowmarks. Sea ice can affect the seafloor to water depths of less than approximately 50 meters. Iceberg erosion, on the other hand, can extend to depths of several hundreds of meters (Jakobsson et al.[2008]).

Widespread findings of glaciogenic bedforms on ridges and plateaus in the central Arctic Ocean suggest that large masses of thick ice covered great parts of this basin several times during the Pleistocene. The findings indicate that most of these features were formed by ice masses grounded on the seafloor rather than by disparate icebergs (Jakobsson et al.[2008]).

## 2.2 The Aim of This Thesis

The aim of this thesis is to investigate possible features of ice shelves in Arctic about 140000 years ago. There are signs on the central Arctic Ocean seafloor of erosion of deep drafting icebergs, which might have come from nearby ice shelves. The extent of ice shelves is not known and in this thesis statistical methods are being used to find reasonable parameters for ice shelves in the Arctic 140000 years ago. Today most ice shelves are found in the Antarctic. Under the presumption that the ice shelves in Antarctic today might have similar features as ice shelves in the Arctic in the past, the Antarctic data are used as plausible relations between the parameters.

## 2.3 Statistical Methods for the Analysis

### 2.3.1 MCMC

Multidimensional computations of the form

$$\boldsymbol{\theta} = E[h(\boldsymbol{X})] = \sum_{j=1}^{\infty} h(\boldsymbol{x_j}) P(\boldsymbol{X} = \boldsymbol{x_j}),$$

with a discrete random vector **X,** with possible values $\mathbf{x}_j$, $j \geq 1$, and probability mass function, $P(\mathbf{X} = \mathbf{x}_j)$ and a function $h(\mathbf{x}_j)$ can be difficult to evaluate. To solve the problem simulations are often being used. A Monte Carlo simulation uses random numbers to generate a sequence of independent and identically distributed random vectors $X_1, X_2, \ldots X_n$ with the mass function $P(\mathbf{X} = \mathbf{x}_j)$. The strong law of large numbers yields

$$\lim_{n\to\infty} \sum_{i=1}^{\infty} \frac{h(\boldsymbol{X})}{n} = \boldsymbol{\theta}$$

and hence $\boldsymbol{\theta}$ can be evaluated when n is sufficiently large (Ross [2000, p.216]).

It can be difficult to draw from the posterior distribution directly, for multidimensional Bayesian models. With Markov Chain Monte Carlo, MCMC, there is a general simulation method that draws values from approximate distributions. The draws are then corrected to better approximate the target posterior distribution. The samples are from a Markov chain and hence the sampled draws only depend on the last value drawn. The approximate distribution converges towards the target distribution and the distribution is thus improving at each step in the simulation. The Markov chain used here is the Gibbs sampler (Gelman et al. [2004, p. 283-287]).

### 2.3.2 The Gibbs Sampler

The Gibbs sampler can be used on the vector **X** where **X** is divided into n components $X_1$, $X_2$, … $X_n$. One component is sampled conditional on all other components of **X**. The Gibbs sampler cycles through the subvectors of **X** and there are n steps in each iteration. The conditional density of **X** is thus

$$p\left(X_i \mid X_j^{t-1}\right), \quad j \neq i,$$

where $X_j^{t-1}$ represents all components of **X,** except $X_i$, at their current values. That is

$$X_j^{t-1} = (X_1^t, X_2^t, \dots, X_{i-1}^t, X_{i+1}^{t-1}, \dots, X_n^{t-1}).$$

Thus the first i-1 components has been updated in iteration t and the components $X_{i+1}^{t-1}, \dots, X_n^{t-1}$ consists of the values from last iteration t-1 and $X_i$ are being sampled conditional on those values (Gelman et al. [2004, p.287-288]).

### 2.3.3 OpenBUGS

The simulations have been performed in OpenBUGS. OpenBUGS is a free of charge program on the internet page www.stat.columbia.edu/~gelman/bugsR. It is a high-level language and the user can specify a model and starting values and the program performs a Markov chain simulation which is automatically implemented for the resulting posterior distribution (Gelman et al. [2004, p. 591]).

There is no prior information about the distributions of the parameters. Using OpenBUGS there is a need for proper prior distributions and hence the parameters are being given proper distributions with large uncertainties (Gelman et al. [2004, p. 593]). This implies that the prior

distribution have a minimal role in the posterior distribution with the aim to let the data speak for themselves (Gelman et al. [2004, p. 61]).

### 2.3.4 Starting Values

The Gibbs sampler should be run long enough to make the starting values unimportant. To make sure that it has been run long enough it is useful to perform several runs with widely dispersed starting values. The conclusions drawn from the different runs should not be sensitive to the choice of the starting values (Spiegelhalter et al. [1996, p. 29]).

It is useful to discard early iterations to decrease the effect of the starting values. Those discarded iterations are called "burn-in" and the length of appropriate burn-in fractions depends on the simulated results (Gelman et al. [2004, p. 295]).

### 2.3.5 The Deviance Information Criterion

To compare the performance of different models it is convenient to measure prediction errors. How well the models fit the data is computed through the deviance, which is defined as

$$D( y ,\theta ) = - 2\log p ( y , \theta ),$$

where y are the data, θ are the population parameters and p is the density function. If the model is normal with constant variance then the deviance is proportional to the mean squared error.

A summary that only depends on y is defined as

$$D_{\hat{\theta}}(y)=D(y, \hat{\theta}(y)),$$

which uses a point estimate for θ, for example the mean of the posterior simulations, to get the minimal deviance. The average discrepancy over the posterior distribution is

$$D_{avg}(y)=E(D(y, \theta) \mid y).$$

Using posterior simulations $\theta_i$ can be estimated by

$$\widehat{D}_{avg}(y)=(1/L)*\sum_{i=1}^{L} D(y, \theta_i).$$

For replicated data $y^{rep}$ the expected deviance can be computed as

$$D_{avg}^{pred}(y)=E [ D (y^{rep}, \hat{\theta} (y))],$$

where

$$D (y^{rep}, \theta) = - 2\log p (y^{rep} \mid \theta)$$

is the expectation averages over the distribution of $y^{rep}$ under the true sampling of the unknown model. $\hat{\theta}$ is a parameter estimate like the posterior mean.

To choose a model with the best out-of-sample predictive power the *deviance information criterion* (DIC) can be computed through

$$\text{DIC}=\widehat{D}_{avg}^{pred}(y) = 2 * \widehat{D}_{avg}(y) - D_{\hat{\theta}}(y),$$

which is an approximation of $D_{avg}^{pred}(y)$ above. The model with the smallest DIC value is the best (Gelman et al. [2004, p. 180-183]).

# 3 Data and Previous Work

### 3.1.1 Data From the Antarctic

The aim here is to find a relation between different variables from the ice shelves in Antarctica. There are no presumptions of a cause and effect relation between the different parameters.

The ice shelves that are considered here are of two different types, open and embayed. An embayed ice shelf is like an ice covered bay and in figure 3.2 it contains the area C and D. An open ice shelf is situated along the coast without a proper bay form. The calving front is the edge of the ice towards the sea water. The points A and B in figure 3.1 and 3.2 are the points where the grounding line meets the calving front. The cordal length is the shortest distance between those points. Other parameters that are being used are the maximal ice thickness at grounding line and the sea water temperature at the calving front. The number of ice rises are also counted and used in the computations. The ice rises are like islands under the ice shelves that are affecting the form of the ice and the ice movements.

| | **Characteristics** |
|---|---|
| L | Length of calving front |
| $L_c$ | Cordal length |
| $P_1$ | Length of grounding line |
| $P_2$ | Maximal ice thickness at grounding line |
| $P_3$ | Number of ice rises |
| $P_4$ | Ice shelf geometry (Class, open=0, embayed=1) |
| $P_5$ | Water temperature at calving front |

Table 3.1.

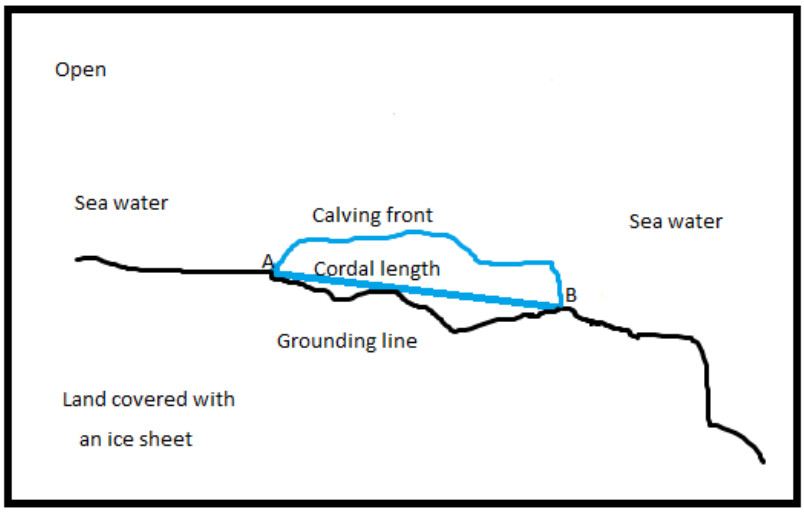


Figure 3.1.

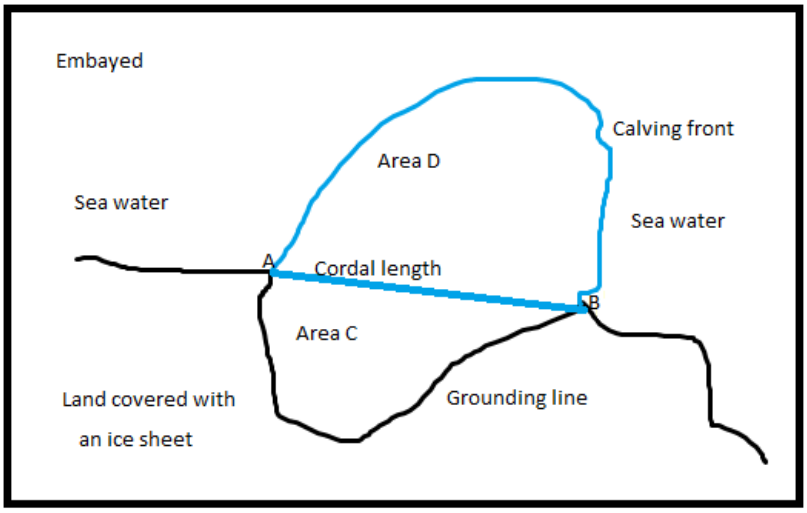


Figure 3.2.

The Antarctic data variables L, $P_1$, $P_2$, $P_3$ and $P_4$ are derived from Bohlander and Scambos' [2007] MODIS Mosaic of Antarctica, together with DiMarzio et al.'s [2007] digital elevation model, which were obtained from observation campaigns of the Geoscience Laser Altimeter System instrument aboard ICESat and an algorithm from Zwally et al.'s [2005] to compute ice-shelf thickness. The ice-fronts and grounding-lines were compiled from satellite imagery and have a resolution of 250 meter and better. The water temperatures, $P_5$, were derived from the World Ocean Circulation Experiment Southern Ocean Data Base [Orsi and Whitworth, 2004].

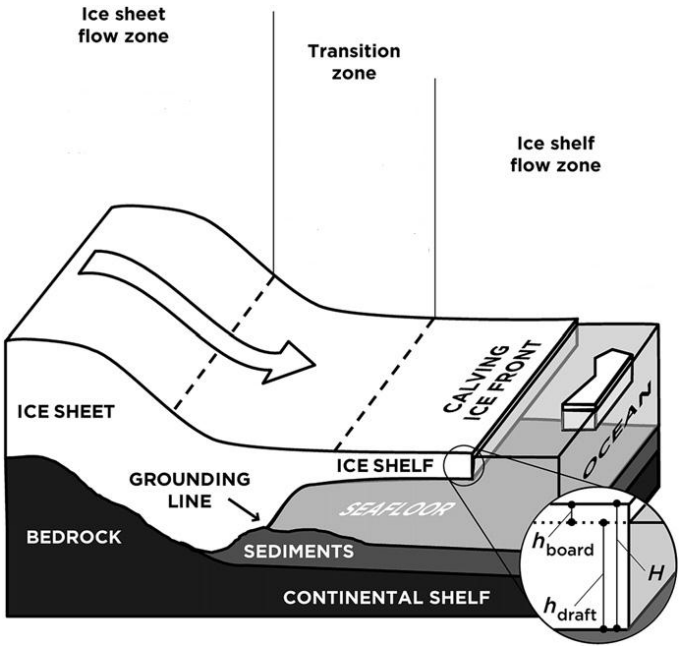


Figure 3.3 from Kirchner et al. [2011].

The coupled ice sheet-ice shelf system can be seen in figure 3.3. Ice on the ground, flow towards the sea, which is depicted with an arrow in the figure. Floating ice shelves fed by large ice sheets get thinner with increasing distance from the grounding line. When the ice shelves are calving it involves the propagation of a fracture through the ice. Icebergs calve from an ice shelf when the thickness is about 200 meters (Jakobsson et al.[2008]) .

### 3.1.2 Data From the Arctic

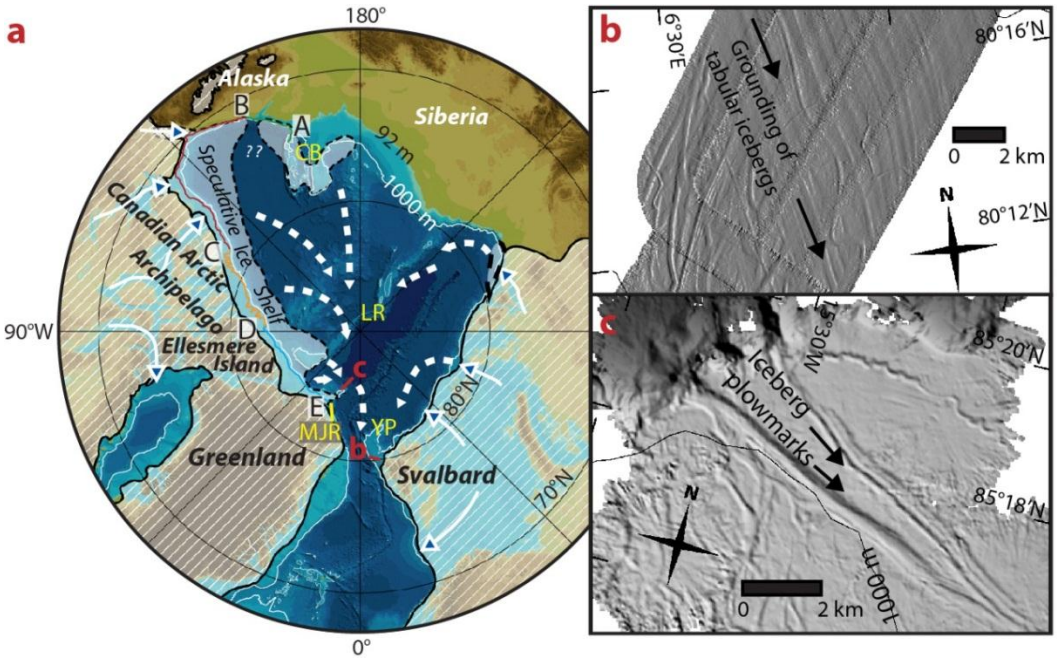


Figure 3.4. Picture from Kirchner et al. [2012].

Like Kirchner et al. [2012] the assumptions are made that the Laurentide ice sheet reached the continental shelf break and that an ice shelf extended from there. The present location of the shelf break is taken as an assumed grounding line for the ice shelf 140000 years ago. This was during a period called MIS 6 (Marine Isotope Stage 6) which extends from 190000 – 130000 years ago. The extent of the ice shelf is not known and five points A-E are depicted in the figure above, along the grounding line, making up possible segments of ice shelves in the statistical analysis. Those assumptions give the values of $P_1$, $P_3$ and $P_4$. The values of $P_2$ and $P_5$ are not known but some plausible values are used in the statistical computations. Like Jakobsson et al. (2010) the sea level in MIS 6 is assumed to be 92 meters below the present sea level (Jakobsson et al. [2010]).

### 3.2 Previous Works

Nina Kirchner et al. [2012] have performed statistical modeling of a former Arctic Ocean ice shelf complex using Antarctic analogies. There are evidence from geophysical mapping and coring of the central Arctic Ocean seafloor that there have been ice sheet/ice shelf complexes during previous glacial periods. There are signs of erosion from deep drafting icebergs. The largest ice shelf complex is believed to have been confined to the Amerasian sector of the Arctic Ocean during Marin Isotope Stage (MIS) 6. To better understand the extent of those ice shelves a statistical analysis is performed to predict configurations of the Arctic Ocean ice shelves based on relations between characteristics from contemporary Antarctic ice shelves. To determine potential sources of deep-draft icebergs extreme value theory is employed. This analysis supports the idea of an extensive MIS 6 ice shelf complex (Kirchner et al. [2012]).

## 4 Antarctic Analysis

### 4.1 Shapes of Ice Shelves

The shapes of ice shelves can have a variety of forms and since it is not known for the ice shelves in the Arctic in MIS 6, certain approximations needs to be done. Inspecting the ice shelves in the Antarctic can give some clues about what shapes are reasonable. The ice shelves in Antarctic are not clearly wider outside the cordal line and hence the ice shelves in the Arctic are assumed not to be broader than the cordal line. It is possible that the ice shelves are thinner further away from the coast. Hence two shapes taking this into account are approximated, a triangle and a rectangle like in figure 4.1.

Inspecting the ice shelves in the Antarctic shows that the triangular and rectangular shapes are simplifications that sometimes have similarities with the real ice shelves but sometimes are different. The ice shelves Shackleton, Amery, Fimbul and Riieser Larsen have a triangular shape, but sometimes the point E in figure 4.1 is more to the left or right. A rectangular shape is seen in Merz and Drygalski ice shelves. Some ice shelves have calving front lengths that are not much larger than the cordal length, for example Filchner, Ronne, Ross and Dotson. Ice shelves with other forms are Ninnis, West and Brunt that could to some extent be seen to have a shape in between a triangular and rectangular shape. Some ice shelves, like Abbot and Getz, have different shapes because of islands interrupting the calving front. Under the present circumstances the triangular and rectangular simplification is acceptable approximation of the MIS 6 Arctic ice shelves.

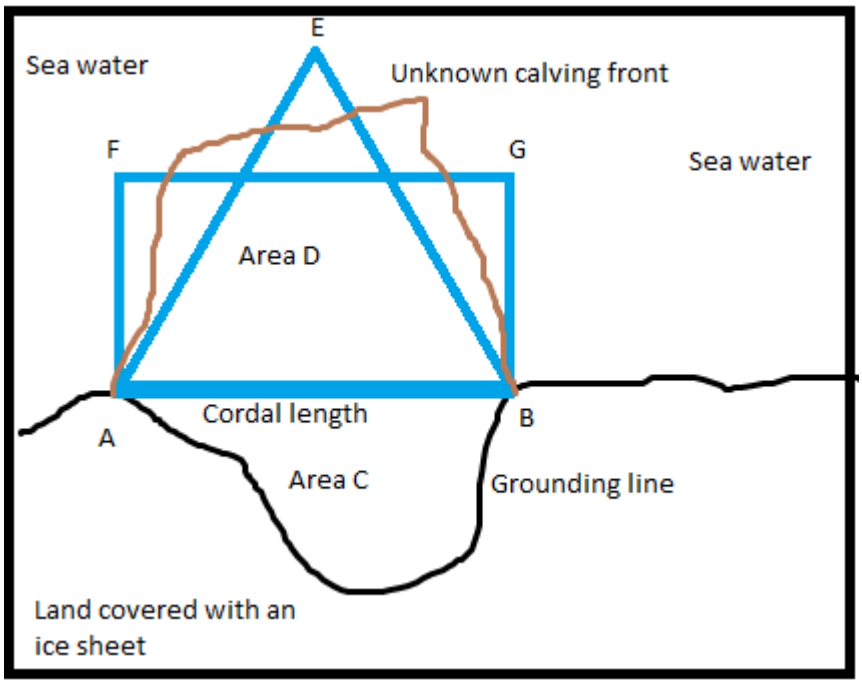


Figure 4.1

Since the approximated calving front using a triangle or rectangle shape are smoother than the true shape a factor called wiggliness is computed. In reality the ice shelf front consist of cape- and bay-like structures. To find an appropriate wiggliness factor the Antarctic ice shelves data are used. The rectangle shape can be thought of as consisting of three line segments outside of the cordal length. In figure 4.1 this would be segments AF, FG and GB. Approximating the Antarctic ice shelves calving fronts with three line segments and four node points has been performed using the first and last points and two points in between. The approximated points F and G are chosen from the 1/3 and 2/3 counts from the file consisting of data from points between A and B along the true calving fronts. The triangle shape can

accordingly be thought of as two line segments outside the cordal line with 3 node points, which are the A, B and E in figure 4.1. Those have been computed for the Antarctic ice shelves using the first, the middle and the last point in the data file.

Those approximations are arbitrary but there are no reasons to believe that other node points would be better approximations of E, F and G, and hence those points are chosen. The wiggliness factor is then computed from dividing the true calving front with the sum of the three line segments for the rectangular shape and the sum of the two line segments for the triangular shape. The result is a number above 1 since the calving front is longer with its cape and bay-like structure.

## 4.2 Wiggliness

Computing the wiggliness for the triangular and the rectangular shape of the ice shelves gives the following histograms and QQplots in figures 4.2 – 4.5.

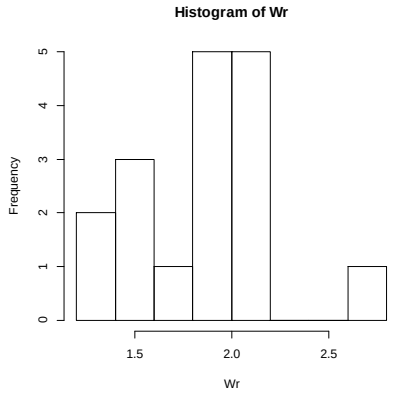


Figure 4.2.

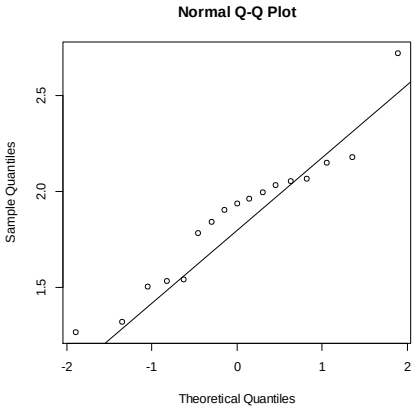


Figure 4.3.

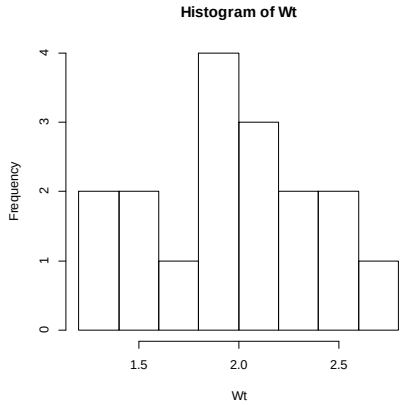


Figure 4.4.

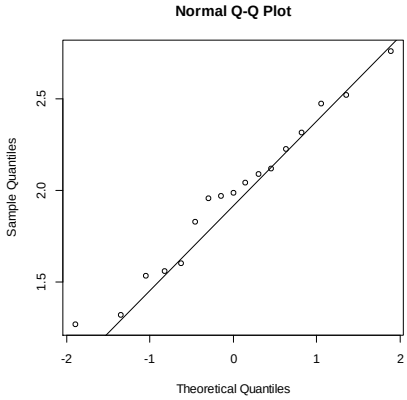


Figure 4.5.

The histograms show that the wiggliness is not very different from the normal distribution and hence the wiggliness is assumed to be approximately normally distributed. $W_r$ is the wiggliness for the rectangular shape and $W_t$ are the wiggliness for the triangular shape.

## 4.3 Method Setup

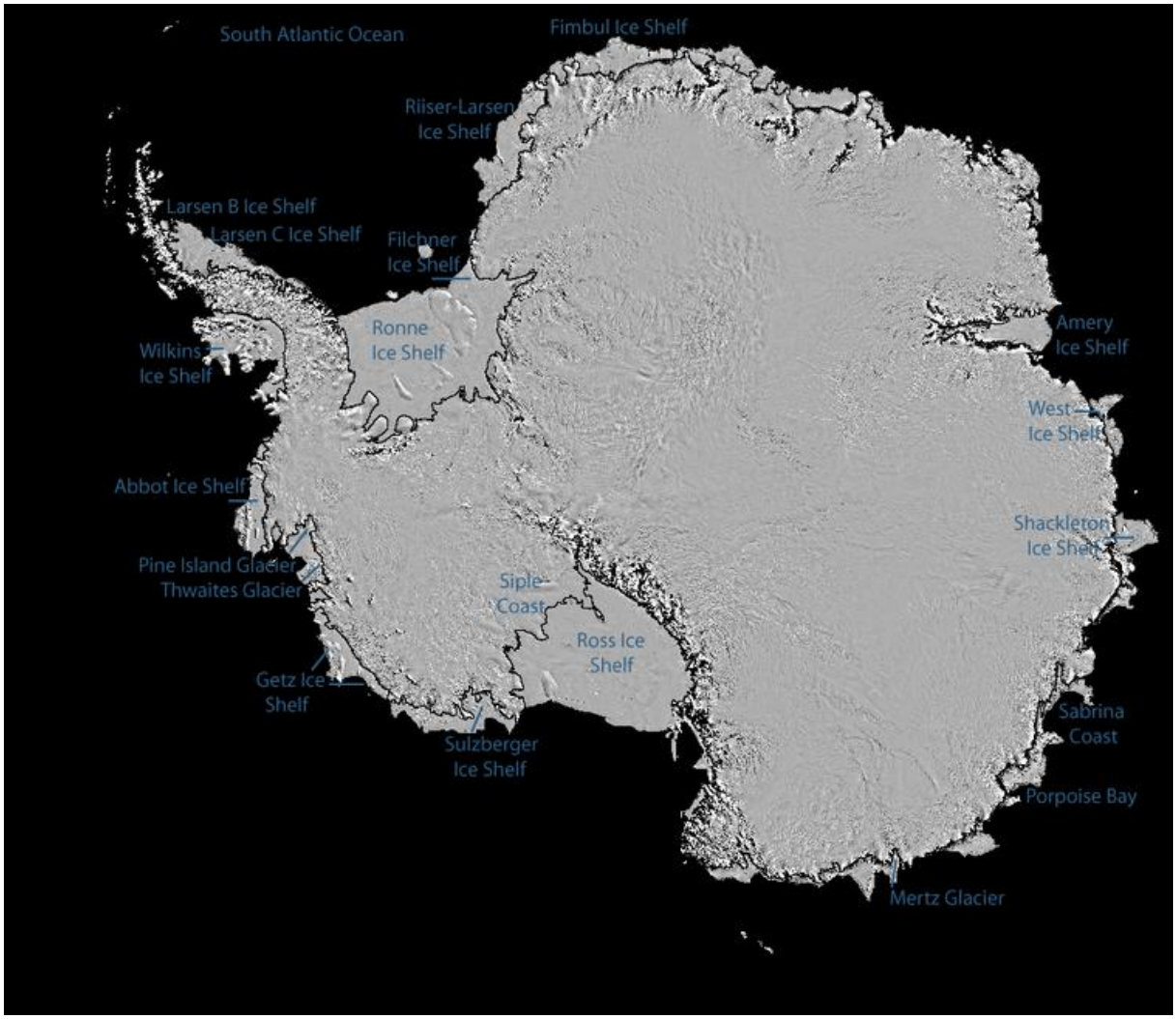


Figure 4.6. The picture is from the Antarctic and comes from http://nsidc.org/.

To get an idea of how the ice shelves are situated and the values of the different parameters, some equations are being used. The length of the calving front in the Antarctic has been computed. The calving front length L can be seen as

$$L=L_1+L_c,$$

where $L_c$ is the cordal length and hence $L_1 \geq 0$. When approximating the true calving length the smooth calving length S is being computed, which can be seen as

$$S=S_1+L_c,$$

and hence $S_1 \geq 0$.

To find reasonable values the wiggliness must be taken into account. The wiggliness is computed from

$$W = L/S,$$

and hence $W \geq 1$.

Together these equations give that

$$L_1 = W*S - L_c = W*(S_1 + L_c) - L_c,$$

and

$$S_1 = L/W - L_c.$$

The wiggliness can hence be written as

$$W = \frac{L_1 + L_c}{S_1 + L_c},$$

and this makes $L_c$

$$L_c = \frac{S_1 * W + L_1}{1 - W}.$$

Different models have been compared to one another to find a good model that shows the relationship between the different parameters and the calving length, L, and the smooth calving length, S, respectively. $\text{Log}(S_1)$ and $\text{Log}(L_1)$ are being used to make sure that the results are being realistic with $L \geq L_c$ and $S \geq L_c$. Standardising $P_j$ around its mean for j=1,…,5 for the parameters, reduces the dependence between $B_{i0}$, $B_{i1}$, … $B_{i5}$, for i=1 or 2, where 1 stands for the regression with the calving length L and 2 stands for the smooth calving length, S. This makes prior independence of the different B values more plausible (Spiegelhalter [1996, p. 27]). The estimate of $B_{i0}$ is more simple and well known when using P minus the arithmetic mean of the values of P, instead of P alone. This makes $B_{i0}$ independent of $B_{i1},\ldots,$ $B_{i5}$. The $B_{i1},\ldots,B_{i5}$ are still the same (Blom et al. [1998, p. 151-152, 227, 246]).

The following model was the best, since it had lowest DIC value and realistic solutions:

$$\begin{aligned} Log(L_1) = B_{10} &+ B_{11}(\mathrm{P}_1 - \mathrm{Mean}(\mathrm{P}_1)) + B_{12}(\mathrm{P}_2 - \mathrm{Mean}(\mathrm{P}_2)) + B_{13}(\mathrm{P}_3 - \mathrm{Mean}(\mathrm{P}_3)) \\ &+ B_{14}(\mathrm{P}_4 - \mathrm{Mean}(\mathrm{P}_4)) + B_{15}(\mathrm{P}_5 - \mathrm{Mean}(\mathrm{P}_5)) \end{aligned}$$

and

$$\begin{aligned} Log(S_1) = B_{20} &+ B_{21}(\mathrm{P}_1 - \mathrm{Mean}(\mathrm{P}_1)) + B_{22}(\mathrm{P}_2 - \mathrm{Mean}(\mathrm{P}_2)) + B_{23}(\mathrm{P}_3 - \mathrm{Mean}(\mathrm{P}_3)) \\ &+ B_{24}(\mathrm{P}_4 - \mathrm{Mean}(\mathrm{P}_4)) + B_{25}(\mathrm{P}_5 - \mathrm{Mean}(\mathrm{P}_5)), \end{aligned}$$

where Log is the natural logarithm. $P_1$-$P_5$ are measured values for the Antarctic.

$\text{Log}(L_1)$ is assumed to be

$$\text{Log}(L_1) \sim \text{N}(\text{Mean}(\text{Log}(L_1)), 0.653),$$

where $\text{Mean}(\text{Log}(L_1))$ is computed in OpenBUGS using the equations above and 0.653 is the computed precision, which is $1/\text{Var}(L_1)$.

Similarly $\text{Log}(S_{r1})$ for the rectangular model is assumed to be

$$\text{Log}(S_{r1}) \sim \text{N}(\text{Mean}(\text{Log}(S_{r1})), 0.123),$$

and $\text{Log}(S_{t1})$ for the triangular model is accordingly assumed to be

$$\text{Log}(S_{t1}) \sim \text{N}(\text{Mean}(\text{Log}(S_{t1})), 0.156).$$

## 4.4 The Antarctic Results

Two sequences with Antarctic data are being performed in order to estimate how long the burn-in period should be. The initial values for the two sequences are chosen to be a bit higher and a bit lower than what could be expected values from doing a test simulation.

### 4.4.1 Rectangular Ice Shelf Shapes in the Antarctic

Two sequences have been simulated with 100 000 burn-in and a total number of 200 000 for each sequence. To decrease the dependence between nearby values in the simulation the results are based on every $10^{th}$ value. Different models have been compared using the DIC value. The best model among those tested was with the following values of $B_{ij}$. The prior have the distribution

$$B_{ij} \sim N(A, Tau),$$

and

$$A \sim N(0, 1),$$

and

$$Tau \sim Ga(0.01, 0.01).$$

$B_{i0}$ have the distribution

$$B_{i0} \sim N(A_{i0}, Tau),$$

where $A_{10}$ is the mean value of $\text{Log}(L_1)$ and $A_{20}$ is the mean value of $\text{Log}(S_1)$ for the rectangular shape.

OpenBUGS simulated the following values with the priors above

| | $B_{10}$ | $B_{11}$ | $B_{12}$ | $B_{13}$ | $B_{14}$ | $B_{15}$ |
|---|---|---|---|---|---|---|
| **Mean** | 5.401 | 0.0001789 | 0.03042 | 0.1604 | -1.524 | -1.013 |
| **Sd** | 0.2217 | 0.0002669 | 0.3941 | 0.1561 | 0.7438 | 1.152 |

Table 4.1.

| | $B_{20}$ | $B_{21}$ | $B_{22}$ | $B_{23}$ | $B_{24}$ | $B_{25}$ |
|---|---|---|---|---|---|---|
| **Mean** | 2.378 | 0.00009641 | 0.1514 | 0.1377 | -2.576 | -1.797 |
| **Sd** | 0.428 | 0.0006124 | 0.7763 | 0.3454 | 1.827 | 2.534 |

Table 4.2.

Those simulations yield the following DIC value:

| | **Dbar** | **Dhat** | **DIC** |
|---|---|---|---|
| **LogL1** | 46.26 | 41.27 | 51.26 |

Table 4.3.

The evaluated parameters $B_{ij}$ from the rectangular shape of the Antarctic ice shelves are then being used to find approximated calving lengths in the Arctic, which could have prevailed in MIS 6.

### 4.4.2 Triangular Ice Shelf Shapes in the Antarctic

A similar simulation as in 4.4.1 has been performed with the triangular ice shelf shape. Different models have been compared using the DIC value. The best model among those tested was with $B_{ij}$ having the same prior distribution as the model for rectangular ice shelf shape.

OpenBUGS simulated the following values with the priors above. The values of $B_{10} - B_{15}$ were the same as for the rectangular variant. The values of $B_{20}$-$B_{25}$ can be seen in table 4.4

| | $B_{20}$ | $B_{21}$ | $B_{22}$ | $B_{23}$ | $B_{24}$ | $B_{25}$ |
|---|---|---|---|---|---|---|
| **Mean** | 1.817 | 0.0002108 | 0.4522 | 0.02747 | -2.636 | -1.934 |
| **Sd** | 0.3878 | 0.0005542 | 0.7174 | 0.3129 | 1.657 | 2.404 |

Table 4.4.

Those simulations yield the following DIC value:

| | **Dbar** | **Dhat** | **DIC** |
|---|---|---|---|
| **LogL1** | 46.26 | 41.27 | 51.26 |

Table 4.5.

Using different initial values gives the same results. The evaluated parameters $B_{i0}$, $B_{i1}$, … $B_{i5}$ from the triangular shape of the Antarctic ice shelves are then being used to find approximated calving lengths in the Arctic, which could have prevailed in MIS 6.

# 5 The Arctic

## 5.1 Ice Shelves in the Arctic in MIS 6

The values of $P_1$, $P_3$ and $P_4$ are known if there actually was an ice shelf there. The values of $P_2$ are not known and in the computations it is assumed that $P_2$ is normally distributed with the same mean and precision as was found in the Antarctic data. The values of $P_5$, the water temperature close to the calving front, are not known. The water temperature close to the ice is not necessarily close to its freezing-point. The freezing-point depends on the content of salt in the water. It could have been different 140 000 years ago. Since there is no information available about those water temperatures, it is assumed that $P_5$ are normally distributed and have the same mean and precision as was found in the Antarctic data. The tested values are given in the appendix. The $B_{ij}$ are assumed to be normally distributed with mean and precision similar to the values from the Antarctic computations.

The approximated ice shelves are seen in table 5.1 where the segments starts and ends in points A-E which can be seen in figure 3.4.

| **Approximated ice shelves are numbered 1-7** | **Segment** |
|---|---|
| | (A-B) |
| 1 | B-C |
| 2 | C-D |
| 3 | D-E |
| 4 | A-C |
| 5 | A-E-embayed |
| 6 | A-E-open |
| 7 | B-E |

Table 5.1.

### 5.1.1 Rectangular Ice Shelf Shapes in the Arctic in MIS 6

With the approximate regression from the Antarctic computations the same model is being used in the Arctic MIS 6 computations. Now is L and S unknown variables and the $B_{ij}$ is approximated from the Antarctic data.

Two sequences of simulations have been performed with 100000 burn-in and a total number of 200000 for each sequence. To decrease the dependence between nearby values in the sequences the results are based on every $10^{th}$ value. The values of $L_1$ and $S_{r1}$ are computed and then added to the cordal length to get the values of L and $S_r$. This is done for the mean and for the $75^{th}$, $90^{th}$ and $95^{th}$ percentile to get an idea of how it might have been.

| Segment | Mean L (km) | L-75% | L-90% | L-95% |
|---|---|---|---|---|
| **1** | 1225,1 | 1448,1 | 1820,8 | 2144,6 |
| **2** | 823,1 | 1087,7 | 1450,9 | 1742,2 |
| **3** | 1000,2 | 1346,2 | 1766,7 | 2126,6 |
| **4** | 1210,3 | 1509,8 | 1921,4 | 2230,4 |
| **5** | 3600,0 | 4472,5 | 5228,0 | 5802,3 |
| **6** | 3914,3 | 4863,8 | 5823,6 | 6564,6 |
| **7** | 2428,6 | 3119,3 | 3794,1 | 4318,7 |

Table 5.2.

| Segment | Mean Sr (km) | Sr-75% | Sr-90% | Sr-95% |
|---|---|---|---|---|
| **1** | 1148,5 | 1151,4 | 1165,8 | 1190,4 |
| **2** | 704,6 | 720,7 | 781,5 | 861,3 |
| **3** | 854,2 | 873,9 | 941,1 | 1030,2 |
| **4** | 1061,7 | 1065,7 | 1083,5 | 1112,7 |
| **5** | 2262,7 | 2275,6 | 2342,2 | 2452,3 |
| **6** | 2267,9 | 2343,5 | 2628,8 | 3037,0 |
| **7** | 1529,3 | 1567,5 | 1703,3 | 1890,0 |

Table 5.3.

Comparing the computed values of L and $S_r$, for the rectangular shape in table 5.2 and 5.3 with the cordal lengths in table 7.8, show that the computed means are not much higher than the cordal lengths. The values of L are higher than $S_r$, which is a sign of the cape- and bay-like structure of the calving length L. This means that the model suggests that the Arctic ice shelves in MIS 6 on average are like Filchner, Ronne, Ross and Dotson ice shelves in the Antarctic.

### 5.1.2 Triangular Ice Shelf Shapes in the Arctic in MIS 6

A similar simulation as in 5.1.1 has been performed with the triangular ice shelf shape. The results can be seen in table 5.4 and 5.5.

| Segment | Mean L | L-75% | L-90% | L-95% |
|---|---|---|---|---|
| **1** | 1225,1 | 1452,6 | 1848,2 | 2162,6 |
| **2** | 826,2 | 1102,2 | 1494,8 | 1800,9 |
| **3** | 1002,3 | 1356,7 | 1818,3 | 2154,9 |
| **4** | 1214,4 | 1531,0 | 1963,6 | 2303,9 |
| **5** | 3737,8 | 4666,2 | 5487,9 | 6055,2 |
| **6** | 4100,9 | 5080,5 | 6135,7 | 7021,9 |
| **7** | 2522,5 | 3257,2 | 3978,1 | 4512,2 |

Table 5.4.

| Segment | Mean St | St-75% | St-90% | St-95% |
|---|---|---|---|---|
| **1** | 1148,5 | 1150,6 | 1161,4 | 1180,5 |
| **2** | 704,6 | 719,0 | 772,2 | 845,2 |
| **3** | 853,8 | 868,2 | 922,5 | 995,2 |
| **4** | 1061,6 | 1064,4 | 1078,0 | 1098,1 |
| **5** | 2262,8 | 2273,6 | 2328,9 | 2427,9 |
| **6** | 2269,4 | 2343,9 | 2625,1 | 3059,0 |
| **7** | 1530,8 | 1573,8 | 1708,2 | 1908,3 |

Table 5.5.

Comparing the mean values of L and $S_t$ in table 5.4 and 5.5 with the cordal lengths in table 7.8 show that the values from the triangular computations lead to similar results as the rectangular computations.

### 5.1.3 Ice Shelf Distance Outside the Cordal Length

For the rectangular shape of the ice shelves the longest orthogonal distance from cordal length to calving front is the same along the ice shelf. It can be computed from

$$Longest\ distance = \frac{S_r - L_c}{2}.$$

The longest orthogonal distance can be seen for different sizes of the ice shelves in table 5.6.

| Segment | Rectangular – Mean Distance (km) | Sr-75% | Sr-90% | Sr-95% |
|---|---|---|---|---|
| **1** | 0,117 | 1,56 | 8,75 | 21,0 |
| **2** | 0,697 | 8,73 | 39,1 | 79,0 |
| **3** | 0,828 | 10,7 | 44,3 | 88,8 |
| **4** | 0,188 | 2,18 | 11,1 | 25,7 |
| **5** | 0,407 | 6,87 | 40,2 | 95,2 |
| **6** | 3,00 | 40,8 | 183,4 | 387,6 |
| **7** | 2,02 | 21,1 | 89,0 | 182,3 |

Table 5.6.

For the triangular shape of the ice shelves the longest orthogonal distance outside the cordal length is the length between the point E and the cordal length in figure 4.1. This can be computed from the Pythagorean theorem with the following equation

$$Longest\ distance = \sqrt{(\frac{S_t}{2})^2 - (\frac{L_c}{2})^2}.$$

The longest orthogonal distance can be seen for different sizes of the ice shelves in table 5.7.

| Segment | Mean distance E-Lc (km) | 75% | 90% | 95% |
|---|---|---|---|---|
| **1** | 11,1 | 36,7 | 86,9 | 136,9 |
| **2** | 22,2 | 75,1 | 159,5 | 234,5 |
| **3** | 23,7 | 82,2 | 176,3 | 256,8 |
| **4** | 13,2 | 40,7 | 94,4 | 141,0 |
| **5** | 31,9 | 115,3 | 277,3 | 441,2 |
| **6** | 92,4 | 307,3 | 666,2 | 1029,7 |
| **7** | 64,9 | 193,9 | 384,5 | 573,4 |

Table 5.7.

## 5.2 Plowmarks From Ice Shelves?

The plowmarks found on the seafloor in the Arctic, which can be seen in figure 3.4 C, might have come from ice shelves about 140 000 years ago. The main part of those

plowmarks lies between point N at 85°19N and 15°30W and the point W at 85°17N and 15°00W.

| Distance between the points (km) | N | W |
|---|---|---|
| A | 2166 | 2172 |
| B | 2476 | 2481 |
| C | 1544 | 1549 |
| D | 870 | 876 |
| E | 179 | 180 |

Table 5.8.

The plowmarks in figure 3.4 C are closest to point E in table 5.8 and if the ice shelf reaches those plowmarks it must reach more than 180 km outside the cordal length from point E, in the right direction. Comparing the distances in table 5.8 with the ice shelves highest orthogonal distances outside the cordal lengths in table 5.6 and 5.7 show that on average the ice shelves do not reach the plowmarks. The segments 1-4 does not reach E and does not reach the plowmarks within the 95$^{th}$ percentile for both shapes of the ice shelves.

For the rectangular shape it needs to be outside the 90$^{th}$ percentile to reach over 180 km from the cordal length. The triangular shape of the ice shelves reach further from the cordal length but that is in the middle of the cordal length, in this model. In reality the highest orthogonal distance need not be in the middle. For the triangular shape it needs to be outside the 75$^{th}$ percentile to reach over 180 km from the cordal length.

# 6 Conclusion

## 6.1 The Model

Using 17 ice shelves from the Antarctic are not an ideal base for the simulations of the Arctic in MIS 6, but can still give some conclusions about possible ice shelves. Ideally there would have been more ice shelves today to investigate. It is also possible that the model could have been more realistic with more variables, but since the MIS 6 data are approximations this would also include more uncertainty. The model would also have been more realistic if the Antarctic and possible Arctic MIS 6 ice shelves had been very similar in size and other

characteristics. There are some crucial differences though, which can be seen in table 7.9 and 7.10. For instance are $P_1$, the grounding line length, much longer in the Arctic data.

If more knowledge about the Arctic during MIS 6 is available in the future a model like this one could make better approximations. It is still valuable to make a statistical analysis to get information about the relationships between the parameters.

## 6.2 The Arctic in MIS 6

Those evaluations suggest that if those plowmarks came from an ice shelf like one of the suggested segment 1 – 7, it must have been an extreme event. This conclusion is in accordance with Kirchner et al. [2012]. The computations here, still suggest that there were ice shelves in the Arctic in MIS 6. This supports the ideas in Kirchner et al. [2011], [2012] and Jakobsson et al. [2008].

Many things might have been different 140000 years ago and we will never know for certain what it was like then. It is still very important to try to understand it better, since the global warming is changing the basis for the ice shelves in the world.

# 7 Appendix

## 7.1 Tables

Below is the parameter data for the different ice shelves in Antarctic.

| | Calving length of front (km) R1 | Area with ice rises(km^2) | len.grounding P1 | max.thick P2 (m) | nr.rises P3 | class P4 | temp P5 |
|---|---|---|---|---|---|---|---|
| **abbot** | 1032 | 47265 | 901 | 1500 | 7 | 0 | -1,3588 |
| **amery** | 473 | 62984 | 2404 | 3000 | 5 | 1 | -1,7184 |
| **brunt** | 664 | 30759 | 471 | 1800 | 0 | 0 | -1,7458 |
| **dotson** | 61 | 4675 | 501 | 2200 | 0 | 1 | -1,6276 |
| **drygalski** | 359 | 2503 | 158 | 4500 | 0 | 0 | -1,83 |
| **ekstrom** | 282 | 7116 | 480 | 1500 | 1 | 1 | -1,8604 |
| **filchner** | 287 | 109271 | 2190 | 2800 | 3 | 1 | -2,0137 |
| **fimbul** | 1075 | 44273 | 893 | 1700 | 6 | 0 | -1,7723 |
| **getz** | 1191 | 46499 | 1154 | 1500 | 8 | 0 | -1,4943 |
| **mertz** | 383 | 5976 | 336 | 2500 | 0 | 0 | -1,5779 |
| **ninnis** | 123 | 1130 | 146 | 2300 | 0 | 1 | -1,7699 |
| **pine.island** | 54 | 3903 | 357 | 3200 | 0 | 1 | -1,0441 |
| **riiser.larsen** | 656 | 48795 | 1256 | 1700 | 4 | 0 | -1,6137 |
| **ronne** | 784 | 333352 | 4796 | 3300 | 5 | 1 | -1,8836 |
| **ross** | 1398 | 488018 | 7011 | 3000 | 6 | 1 | -1,7308 |
| **shackleton** | 946 | 35831 | 960 | 3300 | 6 | 0 | -1,2901 |
| **west** | 784 | 17194 | 618 | 3000 | 2 | 0 | -1,6274 |

Table 7.1. Antarctic data.

The coordinate of the first and last point of cordal lengts for each shelf ice in the Antarctic

| Ice Shelf | Longitude | Latitude | Longitude | Latitude |
|---|---|---|---|---|
| **Abbot_Middle** | -95.598240 | -72.071003 | -91.707152 | -72.619902 |
| **Abbot_North** | -90.748507 | -72.742104 | -89.436204 | -72.637927 |
| **Abbot_South** | -102.82001 | -72.709191 | -102.276320 | -72.142008 |
| **Amery** | 70.195033 | -68.495706 | 73.837546 | -69.748496 |
| **Brunt** | -26.64608 | -76.09656 | -21.97376 | -74.11787 |
| **Dotson** | -113.4089 | -74.16670 | -111.9007 | -74.22683 |
| **Drygalski** | 162.2183 | -75.39061 | 162.5725 | -75.23853 |
| **Ekstrom** | -9.984030 | -70.91713 | -6.445185 | -70.43917 |
| **Filchner** | -44.03762 | -78.17137 | -36.04372 | -78.24080 |
| **Fimbul** | -2.803716 | -70.30025 | 7.413689 | -70.20688 |
| **Getz_Middle** | -124.0231 | -73.85505 | -123.3510 | -73.83482 |
| **Getz_North** | -120.3609 | -73.81301 | -115.1308 | -74.09055 |
| **Getz_South** | -134.7494 | -74.60528 | -127.2728 | -73.72063 |
| **Mertz** | 144.6262 | -67.18135 | 145.2665 | -67.51422 |
| **Ninnis** | 147.0648 | -68.03875 | 147.7238 | -68.33795 |
| **Pine_Island** | -101.7739 | -75.08188 | -101.2547 | -74.72380 |
| **Riiser_Larsen** | -20.62983 | -73.58754 | -12.02715 | -71.66927 |
| **Ronne** | -61.35003 | -74.54698 | -47.67821 | -77.80562 |
| **Ross** | 164.4248 | -78.08109 | -158.6348 | -77.87123 |
| **Shackleton** | 94.92873 | -66.46938 | 102.53313 | -65.88458 |
| **West** | 81.35531 | -67.79402 | 88.74336 | -66.77740 |

Table 7.2. Coordinates for the ice shelves in the Antarctic.

| Ice shelf | Cordal length in km |
|---|---|
| **Abbot Middle** | 145.3 |
| **Abbot North** | 45.1 |
| **Abbot South** | 65.9 |
| **Amery** | 201.3 |
| **Brunt** | 258.2 |
| **Dotson** | 46.4 |
| **Drygalski** | 19.7 |
| **Ekstrom** | 141.2 |
| **Filchner** | 182.5 |
| **Fimbul** | 385.1 |
| **Getz_Middle** | 21.0 |
| **Getz_North** | 164.3 |
| **Getz_South** | 248.1 |
| **Mertz** | 46.2 |
| **Ninnis** | 43.1 |
| **Pine_Island** | 42.7 |
| **Riiser_Larsen** | 357.3 |
| **Ronne** | 512.8 |
| **Ross** | 845.5 |
| **Shackleton** | 348.8 |
| **West** | 337.8 |

Table 7.3. Cordal length for the ice shelves in Antarctic.

In table 7.4 is a table of the Wiggliness for the ice shelves in Antarctic.

| Ice shelf | Wiggliness triangle | Wiggliness rectangle |
|---|---|---|
| Abbot | 2.3138 | 2.1804 |
| Amery | 1.9878 | 1.9618 |
| Brunt | 2.2275 | 2.0333 |
| Dotson | 1.3198 | 1.3199 |
| Drygalski | 2.0408 | 1.9962 |
| Ekstrom | 1.9686 | 1.8434 |
| Filchner | 1.5595 | 1.5403 |
| Fimbul | 2.7604 | 2.7207 |
| Getz | 1.9582 | 1.9034 |
| Mertz | 2.0869 | 2.0654 |
| Ninnis | 2.5195 | 2.1497 |
| Pine Island | 1.2683 | 1.2685 |
| Riiser Larsen | 1.8264 | 1.7854 |
| Ronne | 1.5333 | 1.5345 |
| Ross | 1.6013 | 1.5043 |
| Shackleton | 2.4744 | 1.9382 |
| West | 2.1167 | 2.0532 |

Table 7.4. Wiggliness (calving length divided by smooth calving line) for the ice shelves in Antarctic.

| | Wiggliness triangle | Wiggliness rectangle |
|---|---|---|
| **Mean** | 1.974306 | 1.870506 |
| **Variance** | 0.1773043 | 0.1773043 |

Table 7.5. The mean and variance of the wiggliness factor in Antarctic.

Figures for the Arctic

| Segment | Length of grounding line P1 in km | Max. thick P2 Approximate figures in m | Number of ice rises P3 | Ice shelf geometry P4 | Water temperature Approximated value °C P5 |
|---|---|---|---|---|---|
| A-B | 1764 | 1000-4500 | 2 | --- | -1.0 - -2.5(3.0) |
| B-C=1 | 5310 | 1000-4500 | 0 | Embayed=1 | -1.0 - -2.5(3.0) |
| C-D=2 | 3606 | 1000-4500 | 0 | open=0 | -1.0 - -2.5(3.0) |
| D-E=3 | 2862 | 1000-4500 | 2 | open=0 | -1.0 - -2.5(3.0) |
| A-C=4 | 7056 | 1000-4500 | 2 | embayed=1 | -1.0 - -2.5(3.0) |
| A-E-e=5 | 13524 | 1000-4500 | 4 | embayed=1 | -1.0 - -2.5(3.0) |
| A-E-o=6 | 13524 | 1000-4500 | 4 | open=0 | -1.0 - -2.5(3.0) |
| B-E=7 | 11778 | 1000-4500 | 2 | Open=0 | -1.0 - -2.5(3.0) |

Table 7.6 Arctic data and approximate figures.

The coordinates for the points in Antarctic are being seen in table 7.7.

| Point | Longitude | Latitude |
|---|---|---|
| **A** | -159:05 | 74:29 |
| **B** | -151:48 | 71:21 |
| **C** | -121:59 | 78:11 |
| **D** | -93:48 | 82:42 |
| **E** | -26:04 | 84:02 |

Table 7.7 Coordinates of the node points where possible ice shelves has been situated.

| Segment | Distance (cordal length) |
|---|---|
| **(A-B)** | (424,7) |
| **B-C** | 1148,3 |
| **C-D** | 703,2 |
| **D-E** | 852,5 |
| **A-C** | 1061,3 |
| **A-E** | 2261,9 |
| **A-E** | 2261,9 |
| **B-E** | 1525,3 |

Table 7.8.The data is given for Cordal lengths for different possible ice shelf segments in the Arctic. Segment A-B is not a probable ice shelf but is part of other segments.

| Antarctic | Mean | Lowest value | Highest value |
|---|---|---|---|
| **L** | 620.7059 | 54 | 1398 |
| **Ice shelf area** | 75855.53 | 1130 | 488018 |
| **P1** | 1448.941 | 146 | 7011 |
| **P2 (km)** | 2.517647 | 1.500 | 4.500 |
| **P3** | 3.117647 | 0 | 8 |
| **P4** | 0.4705882 | 0 | 1 |
| **P5** | -1.644635 | -2.0137 | -1.0441 |

Table 7.9. The table shows the highest, lowest and mean values of different parameters in the Antarctic.

| Arktis | Mean | Lowest value | Highest value |
|---|---|---|---|
| **P1** | 8237.143 | 2862 | 13524 |
| **P3** | 2 | 0 | 4 |
| **P4** | 0.4285714 | 0 | 1 |

Table 7.10. The table shows the highest, lowest and mean value of different parameters in the Arctic.

## 7.2 Computer code

### 7.2.1 The Antarctic

The following computer code is the structure that has been used when computing the S1 and L1 for the Antarctic data. Here is the triangular variant.

```
model
{
for (i in 1:N){
LogL1[i]~dnorm(MuLogL1[i], 0.6526984)
MuLogL1[i]<-B10 + B11*(P1[i]-MeanP1) + B12*(P2[i]-MeanP2) + B13*(P3[i]-
3.117647)+ B14*(P4[i]-0.4705882)+B15*(P5[i]- -1.644635)
LogSt1[i]~dnorm(MuLogSt1[i], 0.1564177)
MuLogSt1[i]<-B20 + B21*(P1[i]-MeanP1) + B22*(P2[i]-MeanP2) + B23*(P3[i]-
3.117647)+ B24*(P4[i]-0.4705882)+B25*(P5[i]- -1.644635)
Lc2[i]~dnorm(MuLc2[i],0.00001903929)
MuLc2[i]<-(Wt*exp(LogSt1[i])-exp(LogL1[i]))/(1-Wt)}

B10~dnorm(5.39801,Tau100)
B11~dnorm(A110,Tau110)
B12~dnorm(A120,Tau120)
B13~dnorm(A130,Tau130)
B14~dnorm(A140,Tau140)
B15~dnorm(A150,Tau150)
Wt~dnorm(1.974306,5.6400211)
A110~dnorm(0,1);
A120~dnorm(0,1);
A130~dnorm(0,1);
A140~dnorm(0,1);
A150~dnorm(0,1);
Tau100~dgamma(0.01,0.01);
Tau110~dgamma(0.01,0.01);
Tau120~dgamma(0.01,0.01);
Tau130~dgamma(0.01,0.01);
Tau140~dgamma(0.01,0.01);
Tau150~dgamma(0.01,0.01);

B20~dnorm(1.818989,Tau200)
B21~dnorm(A210,Tau210)
B22~dnorm(A220,Tau220)
B23~dnorm(A230,Tau230)
B24~dnorm(A240,Tau240)
B25~dnorm(A250,Tau250)
A210~dnorm(0,1);
A220~dnorm(0,1);
A230~dnorm(0,1);
A240~dnorm(0,1);
A250~dnorm(0,1);
Tau200~dgamma(0.01,0.01);
```

```
Tau210~dgamma(0.01,0.01);
Tau220~dgamma(0.01,0.01);
Tau230~dgamma(0.01,0.01);
Tau240~dgamma(0.01,0.01);
Tau250~dgamma(0.01,0.01);}

#Data:
list(
N=17,
P1=c(901, 2404, 471, 501, 158, 480, 2190, 893, 1154, 336, 146, 357, 1256, 4796, 7011,
960, 618),
MeanP1=1449,
P2=c(1.500, 3.000, 1.800, 2.200, 4.500, 1.500, 2.800, 1.700, 1.500, 2.500, 2.300, 3.200,
1.700, 3.300, 3.000, 3.300, 3.000),
MeanP2=2.517,
P3=c(7, 5, 0, 0, 0, 1, 3, 6, 8, 0, 0, 0, 4, 5, 6, 6, 2),
P4=c(0, 1, 0, 1, 0, 1, 1, 0, 0, 0, 1, 1, 0, 1, 1, 0, 0),
P5=c(-1.3588, -1.7184, -1.7458, -1.6276, -1.83, -1.8604, -2.0137, -1.7723, -1.4943, -
1.5779, -1.7699, -1.0441, -1.6137, -1.8836, -1.7308, -1.2901, -1.6274),
LogL1=c(6.378901, 5.604699, 6.005860, 2.681022, 5.826885, 4.947340, 4.649187,
6.536547,
6.400888, 5.819489, 4.380776, 2.424803, 5.699440, 5.602857, 6.314453, 6.392252,
6.100767),
LogSt1=c(1.1939225, 3.5929191, 3.7108855, -2.7806209, 5.0515917, 0.9707789,
0.8458683, 1.7715568, 2.9750192, 4.9233693, 1.7625023, -4.1997051, 1.1724821, -
0.5798185, 3.4384932, 3.5516269, 3.5219390),
Lc2=c(442.72,
201.61,257.21,46.156,19.639,140.61,181.71,383.55,588.62,46.065,42.992,42.563,355.94,
510.76, 841.87,347.45,336.53))
```

### 7.2.2 The Arctic

The following computer code is the structure that has been used when computing the $S_1$ and $L_1$ for the Arctic data for the triangular shape.

```
model
{
for (i in 1:N){
LogL1[i]~dnorm(MuLogL1[i], 0.6526984)
MuLogL1[i]<-B10 + B11*(P1[i]- 8237.143) + B12*(P2- 2.517647) + B13*(P3[i]-2)+
B14*(P4[i]- 0.4285714)+B15*(P5- -1.644635)
LogSt1[i]~dnorm(MuLogSt1[i],0.1564177)
MuLogSt1[i]<-B20 + B21*(P1[i]- 8237.143) + B22*(P2- 2.517647) + B23*(P3[i]-2)+
B24*(P4[i]- 0.4285714)+B25*(P5- -1.644635)
Lc[i]~dnorm(MuLc[i],0.000002434303)
MuLc[i]<-(Wt*exp(LogSt1[i])-exp(LogL1[i]))/(1-Wt)}

B10~dnorm(5.401,20.34551)
B11~dnorm(0.0001789,14037920)
B12~dnorm(0.03042,6.438536)
```

```
B13~dnorm(0.1604,41.03876)
B14~dnorm(-1.524,1.807539)
B15~dnorm(-1.013,0.7535204)
Wt~dnorm(1.974306,5.6400211)
P2~dnorm(2.517647, 1.390735)
P5~dnorm(-1.644635,2.0784299)

B20~dnorm(1.817, 6.649430)
B21~dnorm(0.0002108, 3255869)
B22~dnorm(0.4522, 1.943020)
B23~dnorm(0.02747,10.21384)
B24~dnorm(-2.636,0.3642126)
B25~dnorm(-1.934,0.1730339)}

list(
N=7,
#kända variabler
P1=c(5310, 3606, 2862, 7056, 13524, 13524, 11778),
P3=c(0, 0, 2, 2, 4, 4, 2),
P4=c(1, 0, 0, 1, 1, 0, 0),
Lc=c(1148.3,703.2,852.5,1061.3,2261.9,2261.9,1525.3))
```

# 8 References


- Blom, G. & Holmquist, B.(1998) *Statistikteori med tillämpningar.* Studentlitteratur, Lund
- Bohlander, J. and T. Scambos (2007), Antarctic coastlines and grounding line derived from MODIS Mosaic of Antarctica (MOA), Boulder, Colorado USA: National Snow and Ice Data Center. Digital media.
- DiMarzio, J., A. Brenner, R. Schutz, C. A. Shuman, and H. J. Zwally (2007), GLAS/ICESat 500 m laser altimetry digital elevation model of Antarctica. Boulder, Colorado USA: National Snow and Ice Data Center. Digital media.
- Fyke, J.G., A.J. Weaver, D. Pollard, M. Eby, L.Carter, and A. Mackintosh (2011), A new coupled ice sheet/climate model: description and sensitivity to model physics under Eemian, Last Glacial Maximum, late Holocene and modern climate conditions. *Geosci. Model Dev.*, 4, 117-136.
- Gelman, A. Carlin, J.B. Stern, H.S. & Rubin D.B. (2004) *Bayesian Data Analysis*, Chapman & Hall, United States of America, Florida
- Jakobsson, M., Polyak, L., Edwards, M., Kleman, J. and Coakley, B. (2008), Glacial geomorphology of the Central Arctic Ocean: the Chukchi Borderland and the Lomonosov Ridge. *Earth Surface Processes and Landforms*, (33), 526-545.
- Jakobsson, M., J. Nilsson, M. O'Regan, J. Backman, L. Löwemark, J.A. Dowdeswell, L. Mayer, L. Polyak, F. Colleoni, L.G. Anderson, G. Björk, D. Darby, B. Eriksson, D. Hanslik, B. Hell, C. Marcussen, E. Sellén, and Å. Wallin (2010), An Arctic Ocean ice shelf during MIS 6 constrained by new geophysical and geological data. *Quat. Sci. Rev*., 29, 3505-3517.
- Kirchner, N., R. Furrer, M. Jakobsson, H. J. Zwally, and J. W. Robbins (2012). Statistical modeling of a former Arctic Ocean ice shelf complex using Antarctic analogies. Submitted to *Journal of Geophysical Research*, DOI:10.1029
- Kirchner, N., K. Hutter, M. Jakobsson, and R. Gyllencreutz (2011). Capabilities and limitations of numerical ice sheet models: a discussion for Earth scientists and modelers. *Quat. Sci. Rev.*, 30, 3691-3704.
- Orsi, A. H., and T. Whitworth III (2004), Hydrographic Atlas of the World Ocean Circulation Experiment (WOCE), in Volume 1: *Southern Ocean International WOCE Project Office*, edited by M. Sparrow, P. Chapman and J. Gould, Southampton, U.K., ISBN 0-904175-49-9, http://wocesoatlas.tamu.edu/

- Ross, S.M.(2000) *Introduction to Probability Model.* Academic Press, San Diego
- Spiegelhalter, D. J. Best, N. G. Gilks, W. R. & Inskip, H. (1996) "Hepatitis B: a case study in MCMC methods", in Gilks, W.R. Richardson, S. & Spiegelhalter, D.J.(ed.) *Markov Chain Monte Carlo In Practice.* Chapman & Hall, Great Britain
- Zwally, H. J., M. B. Giovinetto, J. Li, H. G. Cornejo, M. A. Beckley, A. C. Brenner, J. L. Saba, and D. Yi (2005), Mass changes of the Greenland and Antarctic ice sheets and shelves and contributions to sea-level rise: 1992-2002, *J Glaciology,* 51(175), 500-527.